Second Harmonic Generation from a Homologous Series of Molecular Crystals: Impact of Supramolecular Interactions

M. Jaya Prakash and T. P. Radhakrishnan*

School of Chemistry, University of Hyderabad, Hyderabad 500 046, India

Received November 26, 2005. Revised Manuscript Received April 14, 2006

Optical second harmonic generation (SHG) from molecular crystals is largely controlled by the molecular hyperpolarizability and the relative disposition of the molecules in the crystal lattice. Even though it is known that intermolecular interactions can modify the bulk SHG, strong and direct influence of such effects in crystals has not been widely demonstrated. We present a new family of crystals based on the achiral remote functionalized nonlinear optical (NLO) chromophore, *N*-(2-aminoethyl)-4-nitroaniline, combined with a homologous series of carboxylic acids, in which the overwhelming impact of supramolecular interactions on the solid-state SHG is clearly manifested. Crystallographic investigations reveal a systematic variation in the superstructure formation of the NLO-phore unit across the series, and the intensities of the SHG from microcrystalline samples are found to correlate with the assembly pattern. Failure of simple additive models in explaining the SHG trend is analyzed using quantum chemical computations of the hyperpolarizability of molecular clusters which establishes the dominant influence of noncovalent intermolecular interactions. The present study illustrates the feasibility of exploiting supramolecular structural features to enhance the NLO response of molecular materials.

Introduction

The significance of molecular materials stems primarily from the flexibility and versatility inherent in their design and fabrication. The structure and properties of these materials can be controlled through fine tuning the synthesis of the molecular building blocks as well as their assembly, mediated by covalent and noncovalent interactions, respectively. The fast and efficient response of molecular materials have made them promising candidates for a number of nonlinear optical (NLO) applications.[1] Quadratic NLO effects such as second harmonic generation (SHG) are sensitive to the structure of the molecules as well as their assembly pattern. In addition to the fundamental requirement of a noncentrosymmetric structure, optimal organization of the molecular NLO-phores is required to elicit efficient SHG response.[2] Extensive research on the design of NLO-phores has led to the delineation of factors that enhance molecular hyperpolarizability, β.[3] Further, a wide range of chemical and physical approaches have been developed to achieve noncentrosymmetric assembly and SHG in bulk materials.[4,5] However, the possible impact of the assembly on the molecular responses is less widely appreciated and established; realization of optimal organizational motifs to achieve maximum bulk SHG from a given NLO-phore remains an important challenge. Computational investigations including a detailed X-ray charge density analysis have shown that supramolecular interactions can considerably alter the hyperpolarizability of molecular NLO-phores;[6,7] several of these studies probe the impact of solvents on molecular β. Earlier work in our laboratory and elsewhere has demonstrated enhanced SHG from helical superstructures.[8] An approach that could provide direct insight into the role of supramo-

* To whom correspondence should be addressed. Phone: 91-40-2301-1068. Fax: 91-40-2301-2460. E-mail: tprsc@uohyd.ernet.in.

(1) (a) Long, N. J. *Angew. Chem., Int. Ed. Engl.* **1995**, *34*, 21. (b) Wolff, J. J.; Siegler, F.; Matschiner, R.; Wortmann, R. *Angew. Chem., Int. Ed. Engl.* **2000**, *39*, 1436. (c) Dalton, L. R. *Pure Appl. Chem.* **2004**, *76*, 1421.

(2) (a) Chemla, D. S., Zyss, J., Eds. *Nonlinear Optical Properties of Organic Molecules and Crystals*; Academic Press: New York, 1987; Vol. 1. (b) Nie, W. *Adv. Mater.* **1993**, *5*, 520. (c) Zyss, J.; Nicoud, J. F. *Curr. Opin. Solid State Mater. Sci.* **1996**, *1*, 533.

(3) (a) Zyss, J.; Ledoux, I. *Chem. Rev.* **1994**, *94*, 77. (b) Kanis, D. R.; Ratner, M. A.; Marks, T. J. *Chem. Rev.* **1994**, *94*, 195. (c) Marks, T. J.; Ratner, M. A. *Angew. Chem., Int. Ed. Engl.* **1995**, *34*, 155.

(4) (a) Lipscomb, G. F.; Garito, A. F.; Narang, R. S. *J. Chem. Phys.* **1981**, *75*, 1509. (b) Eaton, D. F. *Science* **1991**, *253*, 281. (c) Ramamurthy, V.; Eaton, D. F. *Chem. Mater.* **1994**, *6*, 1128. (d) Hoss, R.; Konig, O.; Kramer-Hoss, V.; Berger, U.; Rogin, P.; Hulliger, J. *Angew. Chem., Int. Ed. Engl.* **1996**, *35*, 1664. (e) Gangopadhyay, P.; Sharma, S.; Rao, A. J.; Rao, D. N.; Cohen, S.; Agranat, I.; Radhakrishnan, T. P. *Chem. Mater.* **1999**, *11*, 466. (f) Gangopadhyay, P.; Radhakrishnan, T. P. *Chem. Mater.* **2000**, *12*, 3362.

(5) (a) Dalton, L. R.; Harper, A. W.; Robinson, B. H. *Proc. Natl. Acad. Sci. U.S.A.* **1997**, *94*, 4842. (b) Shi, Y.; Zhang, C.; Zhang, H.; Bechtel, J. H.; Dalton, L. R.; Robinson, B. H.; Steier, W. H. *Science* **2000**, *288*, 119.

(6) (a) Mikkelsen, K. V.; Luo, Y.; Ågren, H.; Jørgensen, P. *J. Chem. Phys.* **1995**, *102*, 9362. (b) Sarma, J. A. R. P.; Rao, J. L.; Bhanuprakash, K. *Chem. Mater.* **1995**, *7*, 1843. (c) Huyskens, F. L.; Huyskens, P. L.; Persoons, A. P. *J. Chem. Phys.* **1998**, *108*, 8161. (d) Ellena, J.; Goeta, A. E.; Howard, J. A. K.; Punte, G. *J. Phys. Chem. A* **2001**, *105*, 8696. (e) Wu, K.; Snijders, J. G.; Lin, C. *J. Phys. Chem. B* **2002**, *106*, 8954. (f) Wang, C.-K.; Wang, Y.-H.; Su, Y.; Luo, Y. *J. Chem. Phys.* **2003**, *119*, 4409. (g) Keinan, S.; Ratner, M. A.; Marks, T. J. *Chem. Mater.* **2004**, *16*, 1848. (h) Bartkowiak, W.; Lipkowski, P. *J. Mol. Model.* **2005**, *11*, 317.

(7) Sainudeen, Z.; Ray, P. C. *J. Phys. Chem. A* **2005**, *109*, 9095.

(8) (a) Kauranen, M.; Verbiest, T.; Boutton, C.; Teerenstra, M. N.; Clays, K.; Schouten, A. J.; Nolte, R. J. M.; Persoons, A. *Science* **1995**, *270*, 966. (b) Deussen, H.-J.; Hendrickx, E.; Boutton, C.; Krog, D.; Clays, K.; Bechgaard, K.; Persoons, A.; Bjùrnholm, T. *J. Am. Chem. Soc.* **1996**, *118*, 6841. (c) Clays, K.; Hendrickx, E.; Verbiest, T.; Persoons, A. *Adv. Mater.* **1998**, *10*, 643. (d) Panda, M.; Chandrasekhar, J. *J. Am. Chem. Soc.* **1998**, *120*, 13517. (e) Gangopadhyay, P.; Radhakrishnan, T. P. *Angew. Chem., Int. Ed.* **2001**, *40*, 2451. (f) Gangopadhyay, P.; Rao, D. N.; Agranat, I.; Radhakrishnan, T. P. *Enantiomer* **2002**, *7*, 119

10.1021/cm052607q CCC: $33.50
Published on Web 05/25/2006

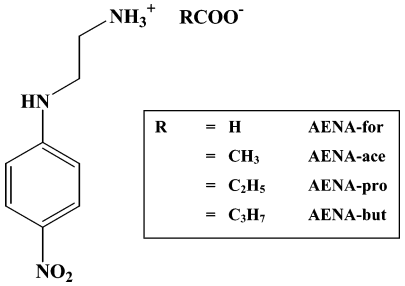

Figure 1. Molecular structure of the salts of AENA investigated.

lecular interactions would be the investigation of crystals of an NLO-phore wherein different superstructures of this unit are induced through the incorporation of a well-defined series of a second molecular component in the lattice, the latter contributing little or nothing to the NLO activity of the material.

We have been investigating SHG active materials based on well-known dipolar, push−pull NLO-phore units, following a general concept of "remote functionalized" systems. The remote functionality is connected by saturated covalent bonds to the π-conjugated chromophore so that it does not modify the response of the NLO-phore appreciably but helps in its organization by effecting strong and directed intermolecular interactions. Remote functionalities on diaminodicyanoquinodimethane[9] and *p*-nitroaniline (pNA)[10] have been exploited to obtain SHG active materials based on achiral building blocks and chiral materials with optimal NLO-phore orientation. We have utilized this approach also to develop materials that exhibit charge transfer exclusively in the solid state[11] and enhanced fluorescence in the solid-state and doped polymer films.[12] Now we have explored a family of molecular crystals based on achiral *N*-(2-aminoethyl)-4-nitroaniline (AENA), formally a remote functionalized derivative of pNA. The homologous series of achiral aliphatic carboxylic acids from formic to butyric was chosen to form salts with AENA (Figure 1). The formate salt (AENA-for) crystallized in a centrosymmetric space group; however, the acetate (AENA-ace), propionate (AENA-pro), and butyrate (AENA-but) salts formed noncentrosymmetric crystals. The latter three show a smooth variation of the solid-state SHG with the response from the acetate being the strongest and that from the butyrate being the weakest. Even though a systematic progression is observed in the relative orientation of the NLO-phore moieties in the three crystals, the bulk SHG predicted based on simple additive models follows a trend opposite to that observed. Interestingly, a well-defined hierarchy exists in the supramolecular organization in these crystals as well, in terms of extended H-bonded chains formed by amino−nitro linked pNA moieties. The superstructure formation involves all the pNA moieties in the acetate salt and only one of the two molecules in the asymmetric unit in the propionate salt, and no such superstructure is formed in the butyrate salt. Quantum chemical computations of hyperpolarizabilities of individual units and molecular clusters establish a clear correlation between the NLO-phore superstructure formation and the solid-state SHG. The significant finding in this study of the family of crystals based on AENA is that rather than the molecular orientations, the supramolecular assembly plays a decisive role in determining the bulk SHG capability; the overwhelming impact of the supramolecular interactions can be visualized as resulting from the modification of the individual NLO-phore responses.

Experimental and Computational Section

Synthesis and Characterization of AENA and Its Salts. AENA was synthesized using the reported procedure[13] of coupling 1,2-diaminoethane and 4-chloronitrobenzene in the presence of copper-(II) chloride. The salts were prepared by adding the carboxylic acid to a solution of 1.0 g (5.52 mmol) of AENA in 50 mL of ethyl acetate at 30 °C followed by stirring for 20 min. The precipitated salts were collected by filtration; specific details and characterization of each salt follow.

AENA-for. A total of 0.25 g (0.21 mL, 5.53 mmol) of formic acid was used; crystals were grown from acetonitrile. Mp 158−160 °C. FT-IR (KBr) $\bar{\nu}$/cm^{-1}: 3290.8, 3194.4, 1602.9, 1556.7, 1381.1, 1286.6, 1107.2. ^{1}H NMR (DMSO-d_6): δ 2.97 (br, 2H), 3.37 (m, 2H), 6.31 (br, 4H), 6.65 (d, 2H), 7.90 (t, 1H), 7.98 (d, 2H). ^{13}C NMR (D_2O): δ 38.21, 39.78, 111.44, 126.80, 137.02, 154.05, 170.91.

AENA-ace. A total of 0.33 g (0.32 mL, 5.54 mmol) of acetic acid was used; crystals were grown by diffusing hexane into an ethyl acetate solution. Mp 124−126 °C. FT-IR (KBr) $\bar{\nu}$/cm^{-1}: 3360.3, 2930.1, 1601.0, 1554.7, 1430.0, 1292.4, 1111.1. ^{1}H NMR (DMSO-d_6): δ 1.80 (s, 3H), 2.83 (br,2H), 3.24 (m, 2H), 5.31 (br, 5H; the two extra protons most likely arise because of traces of moisture interacting with the ammonium group), 6.64 (d, 2H), 7.74 (t, 1H), 7.97 (d, 2H). ^{13}C NMR (D_2O): δ 23.27, 38.25, 39.84, 111.49, 126.83, 137.08, 154.08, 181.33.

AENA-pro. A total of 0.42 g (0.42 mL, 5.63 mmol) of propionic acid was used, and the solution was heated at 70 °C for 10 min and stirred for 30 min; crystals were grown from acetonitrile. Mp 119−121 °C. FT-IR (KBr) $\bar{\nu}$/cm^{-1}: 3350.6, 2912.7, 1602.9, 1554.7, 1394.6, 1277.0, 1105.3. ^{1}H NMR (DMSO-d_6): δ 0.97 (t, 3H), 2.12 (q, 2H), 2.82 (br, 2H), 3.23 (m, 2H), 4.72 (br, 6H; the three extra protons most likely arise because of traces of moisture interacting with the ammonium group), 6.65 (d, 2H), 7.67 (t, 1H), 7.99 (d, 2H). ^{13}C NMR (D_2O): δ 10.17, 30.67, 38.23, 39.83, 111.43, 126.79, 136.95, 154.06, 184.79.

AENA-but. A total of 0.49 g (0.51 mL, 5.58 mmol) of *n*-butyric acid was used, and the solution was heated at 70 °C for 20 min and stirred for 30 min; crystals were grown by diffusing hexane into an ethyl acetate solution. Mp 114−116 °C. FT-IR (KBr) $\bar{\nu}$/cm^{-1}: 3335.2, 3285.0, 2968.7, 1606.8, 1510.4, 1410, 1275.1, 1107.2. ^{1}H NMR (DMSO-d_6): δ 0.86 (t, 3H), 1.50 (sx, 2H), 2.07 (t, 2H), 2.87 (br, 2H), 3.27 (m, 2H), 5.98 (br, 4H; the extra proton most likely arises because of traces of moisture interacting with the ammonium group), 6.66 (d, 2H), 7.85 (t, 1H), 8.00 (d, 2H). ^{13}C NMR (DMSO-d_6): δ 13.73, 18.46, 37.32, 39.20, 43.65, 110.76, 126.07, 135.71, 154.54, 175.73.

Crystallography. X-ray diffraction data were collected on a Bruker Nonius Smart Apex diffractometer (with a charge-coupled device detector). Mo Kα radiation with a graphite crystal monochromator in the incident beam was used. Data were reduced using

(9) (a) Jayanty, S.; Gangopadhyay, P.; Radhakrishnan, T. P. *J. Mater. Chem.* **2002**, *12*, 2792. (b) Jayanty, S.; Radhakrishnan, T. P. *Chem.—Eur. J.* **2004**, *10*, 2661.
(10) Prakash, M. J.; Radhakrishnan, T. P. *Cryst. Growth Des.* **2005**, *5*, 1831.
(11) Jayanty, S.; Radhakrishnan, T. P. *Chem. Mater.* **2001**, *13*, 2072.
(12) Jayanty, S.; Radhakrishnan, T. P. *Chem.—Eur. J.* **2004**, *10*, 791.
(13) Linsker, F.; Evans, R. L. *J. Org. Chem.* **1945**, *10*, 283.

Table 1. Crystallographic Data for AENA-for, AENA-ace, AENA-pro, and AENA-but

	AENA-for	AENA-ace	AENA-pro	AENA-but
empirical formula	$C_9H_{13}N_3O_4$	$C_{10}H_{15}N_3O_4$	$C_{11}H_{17}N_3O_4$	$C_{12}H_{19}N_3O_4$
crystal system	orthorhombic	monoclinic	monoclinic	monoclinic
space group	*Pbca*	*Pc*	*Pn*	*Pc*
a, Å	12.2752(13)	5.608(3)	10.3601(8)	4.8677(5)
b, Å	8.2530(8)	11.314(5)	12.1853(9)	12.5586(13)
c, Å	22.052(2)	9.573(5)	10.5378(8)	11.3875(12)
β, deg	90.00	101.784(8)	101.082(2)	99.521(2)
V, Å^3	2234.0(4)	594.6(5)	1305.50(17)	686.55(12)
Z	8	2	4	2
ρ_{calcd}, g cm^{-3}	1.351	1.348	1.299	1.303
μ, mm^{-1}	0.108	0.105	0.100	0.099
temperature, K	298(2)	298(2)	298(2)	298(2)
λ, Å	0.710 73	0.710 73	0.710 73	0.710 73
no. of reflections	1426	1923	4065	3185
no. of parameters	165	171	359	189
min, max transmission	0.778, 0.988	0.536, 0.998	0.807, 0.997	0.724, 0.992
GOF	1.014	0.985	1.035	1.028
R [for $I \geq 2\sigma_I$]	0.0489	0.0542	0.0506	0.0596
wR^2	0.1027	0.0813	0.1065	0.1251
largest difference peak, hole (e Å^{-3})	0.15, −0.14	0.12, −0.13	0.13, −0.15	0.17, −0.14

SAINT; all non-hydrogen atoms were found using the direct method analysis in SHELXTL and after several cycles of refinement, positions of the hydrogen atoms were calculated and added to the refinement process.[14] Details of data collection, solution, and refinement, as well as the crystallographic information files, are located in Supporting Information.

SHG Measurement. SHG from microcrystalline powders was examined using the Kurtz−Perry[15] method. Particle sizes were graded using standard sieves; sizes ranging from 40 to 300 μm were studied. Samples were loaded in glass capillaries having an inner diameter of 600 μm. The fundamental beam (1064 nm) of a Q-switched nanosecond-pulsed (6 ns, 10 Hz) Nd:YAG laser (Spectra Physics model INDI-40) was used. The second harmonic signal was collected using appropriate optics and detected using a monochromator, photomultiplier tube, and oscilloscope (Tektronix model TDS 210, 60 MHz). Filters were used to bring the signals from all the samples into the same range. Urea with particle size of ∼150 μm was used as the reference. Calibration measurements were carried out using *N*-4-nitrophenyl-(*S*)-prolinol.

Computations. Geometries of the molecules and molecular clusters for the computations were taken from the crystal structure, and hydrogen atoms alone were optimized using the semiempirical AM1 method[16] in the program suite MOPAC93.[17] Static hyperpolarizability, β_0, was computed using (i) AM1 with the TDHF method[18] in MOPAC93 and (ii) ab initio HF/6-31G* with the finite field method in the Gaussian 03 program.[19] The values reported are the magnitude of β_{vec}, conventionally defined using the *x*, *y*, and *z* projections of the various tensorial components. Computations on the protonated AENA showed that it could be treated essentially as a molecule with one dominant β tensor component along the dipole direction defined by the amino and nitro nitrogen atoms. Further details about the computations including the values of $\beta_{1.17}$ (for an excitation wavelength of 1064 nm) from the semiempirical computations are presented in Supporting Information.

Results and Discussion

Crystal structures of AENA[20] and its salt with (*S*)-10-camphorsulfonic acid[10] have been reported previously. We have now synthesized the salts of AENA with counterions ranging from formate to butyrate and investigated their structure; the basic crystallographic data for the four salts are collected in Table 1. AENA-for belongs to the centrosymmetric orthorhombic space group *Pbca* with one molecule in the asymmetric unit. The molecular structure is shown in Figure 2a. The notable feature of the AENA structure is the gauche conformation of the ethylenediamine chain which facilitates double H-bonding with the oxygen atoms of the formate ion. The crystal structure reveals extended H-bonding interactions mediated by the formate ions and centrosymmetric packing of the pNA moieties in AENA. As expected from the symmetry of the lattice, no SHG is observed in the material.

The utility of remote functionalities in assembling noncentrosymmetric crystal lattices from achiral components[9] is once again illustrated by the acetate, propionate, and butyrate salts which are found to belong to the monoclinic space groups *Pc*, *Pn*, and *Pc*, respectively (Table 1). This family of crystals displays interesting similarities and contrasts between the different structures. They exhibit clear hierarchies in the molecular and supramolecular structures and systematic trends in the molecular orientations across the series. The variations are directly or indirectly prompted by the increasing chain length of the carboxylate anions, the only moiety changing across the family. Utilizing the amino

(14) (a) *SAINT-Plus*, Version 6.45; Bruker AXS: Madison, WI, 2003. (b) *SHELXTL*, Version 6.14; Bruker AXS: Madison, WI, 2003.
(15) Kurtz, S. K.; Perry, T. T. *J. Appl. Phys.* **1968**, *39*, 3798.
(16) Dewar, M. J. S.; Zoebisch, E. G.; Healy, E. F.; Stewart, J. J. P. *J. Am. Chem. Soc.* **1985**, *107*, 3902.
(17) *MOPAC93*; Fujitsu, Inc.: Tokyo, 1993.
(18) Dupuis, M.; Karna, S. *J. Comput. Chem.* **1991**, *12*, 487.
(19) Frisch, M. J.; Trucks, G. W.; Schlegel, H. B.; Scuseria, G. E.; Robb, M. A.; Cheeseman, J. R.; Montgomery, J. A., Jr.; Vreven, T.; Kudin, K. N.; Burant, J. C.; Millam, J. M.; Iyengar, S. S.; Tomasi, J.; Barone, V.; Mennucci, B.; Cossi, M.; Scalmani, G.; Rega, N.; Petersson, G. A.; Nakatsuji, H.; Hada, M.; Ehara, M.; Toyota, K.; Fukuda, R.; Hasegawa, J.; Ishida, M.; Nakajima, T.; Honda, Y.; Kitao, O.; Nakai, H.; Klene, M.; Li, X.; Knox, J. E.; Hratchian, H. P.; Cross, J. B.; Bakken, V.; Adamo, C.; Jaramillo, J.; Gomperts, R.; Stratmann, R. E.; Yazyev, O.; Austin, A. J.; Cammi, R.; Pomelli, C.; Ochterski, J. W.; Ayala, P. Y.; Morokuma, K.; Voth, G. A.; Salvador, P.; Dannenberg, J. J.; Zakrzewski, V. G.; Dapprich, S.; Daniels, A. D.; Strain, M. C.; Farkas, O.; Malick, D. K.; Rabuck, A. D.; Raghavachari, K.; Foresman, J. B.; Ortiz, J. V.; Cui, Q.; Baboul, A. G.; Clifford, S.; Cioslowski, J.; Stefanov, B. B.; Liu, G.; Liashenko, A.; Piskorz, P.; Komaromi, I.; Martin, R. L.; Fox, D. J.; Keith, T.; Al-Laham, M. A.; Peng, C. Y.; Nanayakkara, A.; Challacombe, M.; Gill, P. M. W.; Johnson, B.; Chen, W.; Wong, M. W.; Gonzalez, C.; Pople, J. A. *Gaussian 03*, revision B.04; Gaussian, Inc.: Pittsburgh, PA, 2003.
(20) Kaida, S.; Wakita, K.; Shimizu, T.; Sonoda, N.; Miki, K.; Kasai, N. *Acta Crystallogr., Sect. C* **1989**, *45*, 2025.

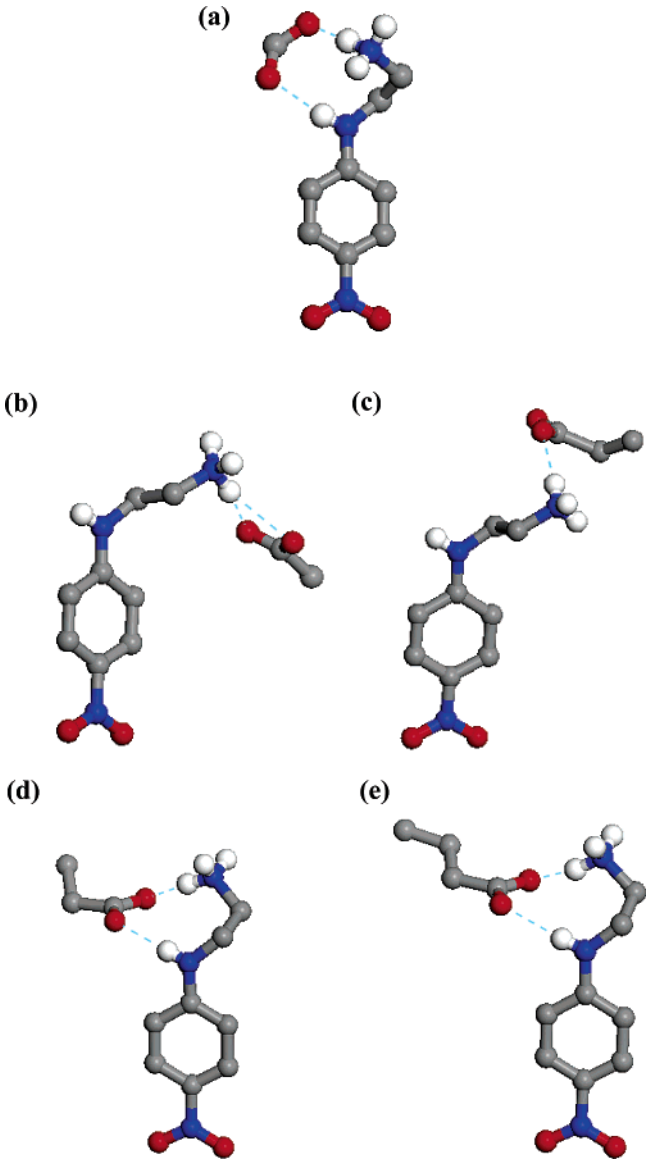

Figure 2. Molecular structures of (a) AENA-for, (b) AENA-ace, (c, d) AENA-pro, and (e) AENA-but from crystal structure analysis; H atoms of only amino and ammonium groups are shown for clarity. C (grey), H (white), N (blue), and O (red) atoms and H-bonds (broken cyan line) are indicated.

groups connected to the aromatic ring as well as the terminal ammonium functionality, the AENAs form a host of intermolecular H-bonds between themselves and with the carboxylate group of the anion in all the crystals. Figure 2 shows the different molecular structures; there is only one formula unit in the asymmetric units of AENA-ace (Figure 2b) and AENA-but (Figure 2e), but there are two in the case of AENA-pro (Figure 2c,d). The counterion is H-bonded to the terminal ammonium group of AENA in the acetate salt and in one of the molecules in the asymmetric unit of the propionate salt (Figure 2b,c). This is facilitated by the anti conformation of the ethylenediamine group on AENA and is accompanied by the formation of extended H-bonded superstructures of the pNA moieties mediated by the aromatic amino and nitro groups. In the case of the second molecule in the asymmetric unit of AENA-pro and the molecule in AENA-but (Figure 2d,e) on the other hand, the ethylenediamine group on AENA has a gauche conformation and forms cyclic structures with the oxygen atoms of the carboxylate counterion through two H-bonds. This structure, similar to that in AENA-for (Figure 2a), effectively precludes extended H-bonded superstructure formation of the pNA moieties through amino−nitro interactions. The involvement of all, half, or none of the pNA moieties in the formation of the extended amino−nitro H-bonded chains in the case of acetate, propionate, and butyrate crystals, respectively, is graphically depicted in Figure 3. The systematic trend in the orientation of the pNA NLO-phore units with respect to the crystallographic axes, from acetate to butyrate, is revealed in the packing diagrams viewed along the crystallographic *c* axis (Figure 4); the specific value of the angles and their relevance will be discussed later. The figure suggests that the increasing length of the carboxylic acid chains causes the tilt of the AENA moieties with respect to the *a* and *b* axes to increase and decrease, respectively; the amino−nitro H-bonds between the pNA moieties facilitated by the molecular orientation in AENA-ace is partially disrupted in AENA-pro and fully disrupted in AENA-but.

The optical absorption spectra of the four AENA salts in solution and in the solid state are collected in Figure 5. Because the chromophore is the same, the solution spectra of all the compounds are nearly identical; the λ_{max} is in the range of 390−398 nm. The solid-state spectra are broader with additional peaks at lower and higher energies resulting from intermolecular excitonic interactions. Significantly, there is a steady shift of the absorption edge (λ_{cutoff}) from the formate to the butyrate salt. The red-shifted peaks are usually attributed to J-type aggregates of chromophores. The trend in the AENA salts possibly arises because of the systematic variation of the angle between adjacent pNA chromophore dipoles in the J-type or a related configuration in the respective crystals, 37.6° in AENA-for, 47.5° in AENA-ace, 52.3 and 87.0° in AENA-pro, and 87.9° in AENA-but. The SHG data on microcrystalline powders of the three salts are displayed in Figure 6. The variation of the SHG with particle size shows that they are all phase-matchable materials. The average saturation values at larger particle sizes, normalized with respect to that of urea (SHG = 1U), are 25.5 U (AENA-ace), 22.0 U (AENA-pro), and 4.1 U (AENA-but). The SHG from the first two are quite appreciable; all materials showed stable SHG and no visible damage up to ∼1 GW/cm^2 of laser power. It is important to note that, even though the possibility of resonance enhancement of the SHG increases from the acetate to the butyrate salt as a result of the λ_{cutoff} tending toward the second harmonic wavelength of 532 nm, the observed SHG follows the opposite trend. We explore below factors which could play an overriding role leading to such effects.

The oriented gas model[21] provides a basis to analyze the SHG of molecular crystals in terms of the contributions of the molecular building blocks and their organization. Within this model, the solid-state NLO response of a crystal results from additive contributions of the NLO-phore units; hence, the SHG of a series of crystals based on the same NLO-phore are controlled by the relative molecular orientations in the lattice. In the case of a lattice with point group *m*

(21) Zyss, J.; Oudar, J. L. *Phys. Rev. A.* **1982**, *26*, 2028.

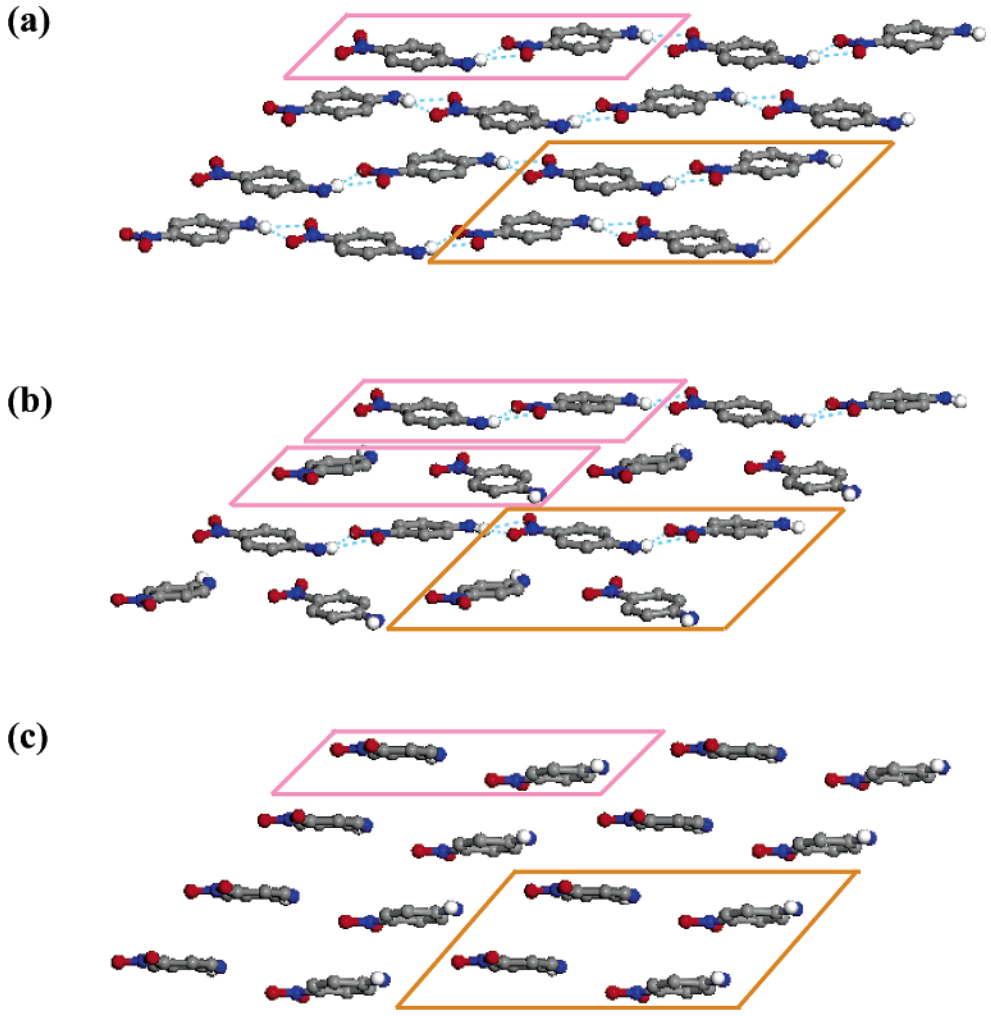

Figure 3. Organization of the pNA moieties in the crystals of (a) AENA-ace, (b) AENA-pro, and (c) AENA-but and formation of amino−nitro H-bonded superstructures in the former two; H atoms of only amino groups are shown for clarity. C (grey), H (white), N (blue), and O (red) atoms and H-bonds (broken cyan line) are indicated. The dimer (in the magenta box) and tetramer (in the orange box) clusters used in the computational studies are specified; the computations used the full protonated AENA and not just the pNA units shown in the figure.

built up of a dipolar NLO-phore, the β tensor of which is dominated by a single large component, the effective quadratic NLO susceptibility coefficients for electro-optic effects and phase-matched SHG are given by $b_{ZZZ}^{\text{eff}} = \sin^3 \theta$ and $b_{ZYY}^{\text{eff}} = \sin \theta \cos^2 \theta$, respectively;[21] θ is the angle between the major β component (usually coincident with the dipole vector) and the crystallographic b axis (assuming ac to be the mirror/glide plane). For such a system, the highest SHG response is obtained at $\theta = 35.26°$ corresponding to the maximum value of $b_{ZYY}^{\text{eff}} = 0.38$. In the three AENA salts, the angle θ may be defined using the dipole vector of the pNA moiety connecting the nitrogen atoms of the amino and nitro groups; the angle is found to be largest in the acetate and smallest in the butyrate salts, and the two molecules in the asymmetric unit of the propionate salt show dispositions similar to that in the other two crystals (Figure 4, Table 2). The angle θ in AENA-but is closest to the ideal one for SHG, and that in AENA-ace is the farthest; AENA-pro lies in between. On the basis of these angles, it is also seen that the effective nonlinear coefficients, b_{ZZZ}^{eff} and b_{ZYY}^{eff}, decrease and increase, respectively, from the acetate to the butyrate salts. The b_{ZZZ}^{eff} values indicate that the electro-optic effect would decrease from AENA-ace to AENA-but. The trends in the angle θ and b_{ZYY}^{eff} suggest that the SHG should be weakest in AENA-ace and strongest in AENA-but. However, this is opposite to the trend observed in the experimental SHG values and indicates that the assumption of similar β for the AENA moiety in the three systems is clearly untenable.

Examination of the crystal structures has shown that the supramolecular structure formation is quite different in the three AENA salts and that they follow a well-defined pattern. To assess the impact of such assemblies on the NLO response, we have carried out quantum chemical computations of the hyperpolarizability of single molecules and clusters observed in the crystals. The monomer in each case is the protonated AENA. In the case of AENA-ace, we have chosen the amino−nitro H-bonded adjacent molecules in the chains as the dimer and the combination of two such dimers from adjacent chains with no direct H-bond link between them as the tetramer (Figure 3a; the figure depicts only the pNA moieties, but the computations are carried out on the protonated AENA). In AENA-pro, two types of dimers exist, one with a H-bond and the other without, and the tetramer is a set containing both (Figure 3b). In AENA-but, the dimer as well as the tetramer do not show any amino−nitro H-bonding (Figure 3c). The values of the static hyperpolarizability computed for the various systems are provided in

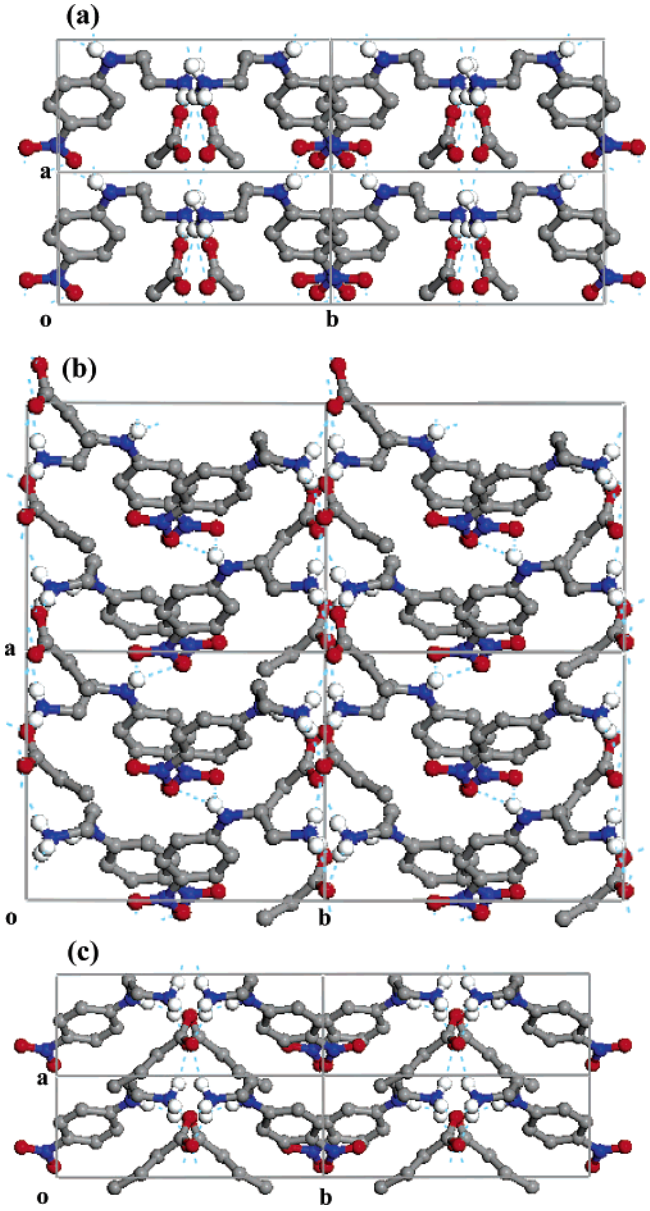

Figure 4. Packing of molecules in the crystals of (a) AENA-ace, (b) AENA-pro, and (c) AENA-but, viewed along the *c* axis; H atoms of only amino and ammonium groups are shown for clarity. C (grey), H (white), N (blue), and O (red) atoms and H-bonds (broken cyan line) are indicated.

Table 3. The trends at the semiempirical and ab initio levels are found to be parallel; we note that $\beta_{1.17}$ (Supporting Information) also follows the same pattern. In the case of AENA-ace, where the pNA moieties form extended amino−nitro H-bonded superstructure, the β_0 per molecule increases by a factor of ∼2.2 from monomer to dimer; this is a direct consequence of the modification of the electronic wave functions due to the supramolecular structure formation. In the traditional picture of push−pull effects, this could be attributed to the increased acceptor and donor strengths respectively of the nitro and amino groups resulting from the intermolecular H-bond interactions. From dimer to tetramer, the β_0 per molecule decreases slightly as a result of the additive effect of tensor components of the two dimers which are aligned at an angle to each other. The observations are rather similar in the case of AENA-pro, except that the increase of average β_0 per molecule from monomer to dimer is by a factor of ∼2.0; this is because the enhancement

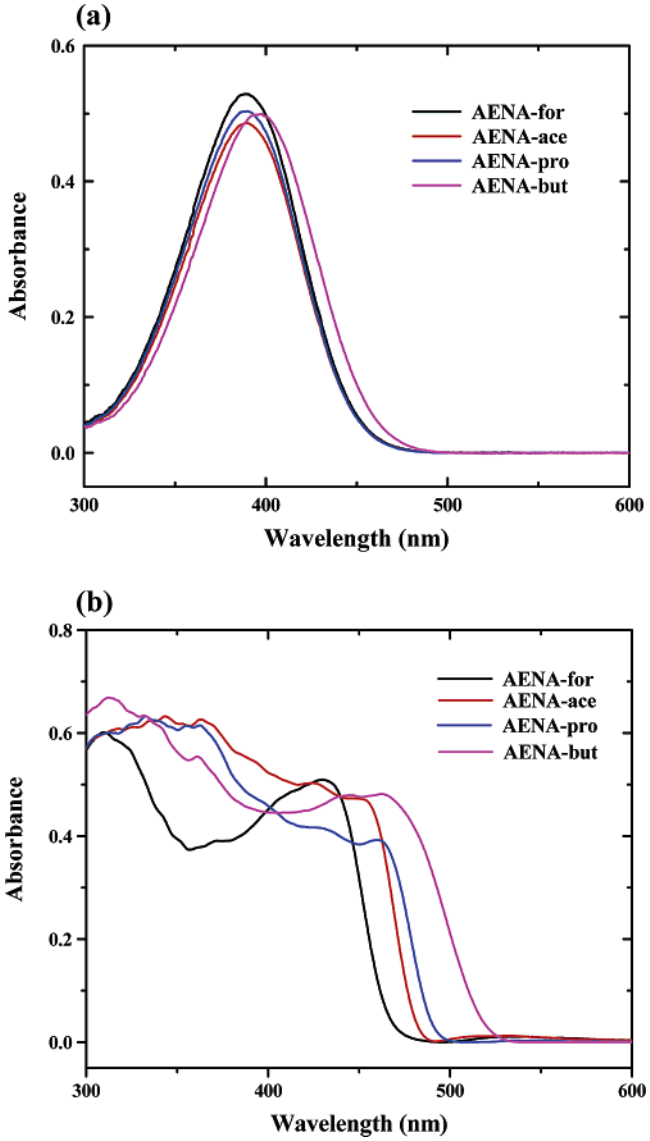

Figure 5. Optical absorption spectra of AENA-for, AENA-ace, AENA-pro, and AENA-but in (a) aqueous solution and (b) the solid state.

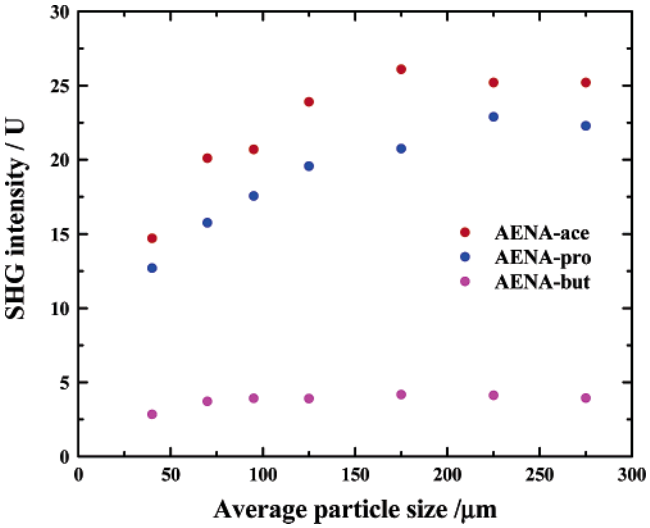

Figure 6. SHG (with respect to that of urea) from microcrystalline powders of AENA-ace, AENA-pro, and AENA-but with different particle sizes.

through H-bonded supramolecular structure formation is applicable only to one of the dimers, the H-bonded dimer

Table 2. Angle, θ, between the Dipole Axis of the pNA Moiety in AENA and the Crystallographic *b* Axis and the Effective Quadratic NLO Susceptibility Coefficients in the Crystals of AENA-ace, AENA-pro, and AENA-but

crystal	θ (deg)	b^{eff}_{ZZZ} (d_{11})	b^{eff}_{ZYY} (d_{12})
AENA-ace	66.2	0.766	0.149
AENA-pro[a]	63.9, 43.5	0.525	0.268
AENA-but	43.9	0.333	0.360

[a] In the propionate salt, the angles for the two molecules in the asymmetric unit are presented, and the effective coefficent is the average value.

Table 3. Computed (AM1/TDHF [HF/6-31G*/FF]) Static Hyperpolarizabilities (β_0) of Protonated AENA and Its Supramolecular Clusters[a] in AENA-ace, AENA-pro, and AENA-but

	β_0 (10^{-30} esu)					
	AENA-ace		AENA-pro[b]		AENA-but	
cluster	cluster	molecule	cluster	molecule	cluster	molecule
monomer	3.062	3.062	3.213,[c] 2.612[d]	2.913	2.042	2.042
	[2.887]	[2.887]	[3.129,[c] 2.001[d]]	[2.565]	[1.621]	[1.621]
dimer	13.640	6.820	15.253,[c] 8.365[d]	5.905	1.182	0.591
	[12.143]	[6.072]	[13.216,[c] 7.060[d]]	[5.069]	[1.076]	[0.538]
tetramer	22.273	5.568	17.353	4.338	5.859	1.465
	[20.331]	[5.083]	[15.925]	[3.981]	[3.424]	[0.856]

[a] The value *per molecule* is also indicated in each case. [b] For AENA-pro, the values for the monomers and dimers which are involved and not involved in the extended amino−nitro H-bonded chains of pNA moieties and average values per molecule are provided. [c] With the amino−nitro H-bond. [d] Without the amino−nitro H-bond.

showing a considerably higher β_0 than the non-H-bonded one. In AENA-but, the β_0 per molecule decreases from monomer to dimer because of the unfavorable orientation of the AENA units in the dimer and absence of any enhancement through a direct H-bond link. There is a small increase on forming the tetramer which possibly is an effect of some π-stacking interactions.[7] The most significant observation in Table 3 is the steady decrease of the effective β_0 per molecule from the acetate to the propionate to the butyrate salt for the dimer and tetramer clusters, even though the values for the monomers change very little. This implies that the supramolecular structure formation directly influences the molecular NLO responses and the intermolecular interactions overwhelm the impact of the NLO-phore orientations on the solid-state SHG of the materials discussed above. These crystals built using the same NLO-phore unit with their organization and superstructure formation tuned by remote changes in the counterion facilitate the unambiguous demonstration of the modification of the solid-state SHG capability through supramolecular effects. Investigations with other families of H-bonding NLO-phore systems would provide insight into the generality of these effects.

The Kurtz−Perry measurement provides only a single measurement of the relative SHG capability of a material; it does not provide detailed information on the specific nonlinear susceptibility tensor components. The utility of the measurement on randomly oriented microcrystalline powder samples is thus limited in terms of probing the application potential of novel materials. It is possible that the strong diagonal nonlinear susceptibility tensor component (d_{11}) of AENA-ace can be exploited if a fundamental laser beam with appropriate polarization and large enough single crystals of the material are employed.

Conclusions

A family of noncentrosymmetic organic salts are developed based on an achiral "remote functionalized" NLO-phore and a homologous series of achiral carboxylate ions. They show a systematic variation of molecular and supramolecular organizational features and, in parallel, solid-state SHG. A simple additive approach to relate the molecular and bulk NLO responses fails, suggesting that intermolecular interactions play a significant role in determining the solid-state SHG. Quantum chemical computations on the supramolecular clusters confirm the overriding impact of cooperative interactions on the molecular hyperpolarizability and provide an explanation for the observed trend in the bulk SHG capabilities. This study suggests that the incorporation of appropriate supramolecular effects in the design can lead to effective exploitation of the molecular NLO response and fabrication of efficient molecular materials for NLO applications.

Acknowledgment. Financial support from the CSIR and DST, New Delhi, use of the National Single Crystal X-ray Diffractometer Facility at the School of Chemistry, and the Universities with Potential for Excellence Programme of the UGC, New Delhi, are acknowledged. M.J.P. thanks the CSIR, New Delhi, for a Senior Research Fellowship. We thank one of the reviewers for making critical suggestions for improving the overall perspective of this paper.

Supporting Information Available: Details of crystal structure determination and computational data (PDF) and crystallographic information files (CIF). This material is available free of charge via the Internet at http://pubs.acs.org.

CM052607Q